

## Dynamics of rifting and modes of extension on icy satellites

F. Nimmo<sup>1</sup>

Department of Earth Sciences, University College London, London, UK

Received 1 August 2003; revised 4 November 2003; accepted 17 November 2003; published 2 January 2004.

[1] A simple numerical model of extension in icy satellite shells is developed. Thinning of the ice weakens the shell, promoting further extension. If lateral flow in the lower part of the shell is unimportant, extension is opposed and wide rifts are generated; if lateral flow is rapid, localized extension is favored and narrow rifts are produced. Thick shells or high strain rates favor the development of narrow rifts; low strain rates favor wide rifting. It is proposed that bands, extensional features on Europa, are narrow rifts, while groove lanes on Ganymede are wide rifts. The existence of wide rifting on Ganymede is consistent with previous estimates of a conductive shell thickness at the time of rifting of 4–8 km and a strain rate of  $<10^{-14} \text{ s}^{-1}$ . Narrow rifting on Europa can be produced at sufficiently high strain rates for a wide range of shell thicknesses. Assuming a pre-rift brittle-ductile transition depth of 0.5–3 km restricts the solutions to relatively thin ( $<15 \text{ km}$ ) shells and high ( $>10^{-15} \text{ s}^{-1}$ ) strain rates at the time of rifting. Whether this shell thickness applies to present-day Europa depends on the age of band formation, which is poorly known. The difference between rifting behavior on Ganymede and Europa is due to either higher strain rates or higher shell thicknesses on Europa during rifting. The mean stresses required to cause the observed rifting are  $\approx 0.2 \text{ MPa}$  for Ganymede and  $\approx 0.3 \text{ MPa}$  for Europa. These values are comparable to estimates derived from flexural

features. **INDEX TERMS:** 5475 Planetology: Solid Surface Planets: Tectonics (8149); 6218 Planetology: Solar System Objects: Jovian satellites; 8109 Tectonophysics: Continental tectonics—extensional (0905); 8160 Tectonophysics: Rheology—general; **KEYWORDS:** Europa, Ganymede, extension, faulting, ice

**Citation:** Nimmo, F. (2004), Dynamics of rifting and modes of extension on icy satellites, *J. Geophys. Res.*, 109, E01003, doi:10.1029/2003JE002168.

### 1. Introduction

[2] On Earth, plate tectonics causes extensional stresses which may result in rifting or the creation of new seafloor and mid-ocean ridges. Both the consequences of extension [McKenzie, 1978] and the balance of forces operating during extension [e.g., England, 1983; Kusznir and Park, 1987; Buck, 1991] have been modeled in great detail for terrestrial settings. A surprising result of the Voyager mission, subsequently confirmed by higher resolution Galileo images, was the existence of extensional features on Jupiter's moons Europa and Ganymede [e.g., Sullivan *et al.*, 1998; Pappalardo *et al.*, 1998]. It will be argued below that these features can be used to constrain the ice shell thickness and strain rate at the time of rifting.

[3] Little work has been done on the dynamics of rifting for icy satellites. Parmentier *et al.* [1982] considered the kinematics of extensional areas on Ganymede, and Helfenstein and Parmentier [1983, 1985] compared the distribution of extensional features on Europa with theoretical stress maps. Golombek and Banerdt [1990] used estimated faulting depths

to constrain the thermal structure of Europa, and Dombard and McKinnon [2001] estimated the strain rate and thermal structure associated with the formation of extensional features on Ganymede. It will be shown below that the results of the latter paper are in good agreement with those obtained here.

[4] In this paper, I adapt a simple technique used for modeling terrestrial rifting [Buck, 1991] to the icy satellite case. I outline some of the main differences between rifting on silicate and icy bodies, and provide possible explanations for why extension is expressed differently on Europa compared to Ganymede. In section 2, the basic observations are discussed. Section 3 outlines the model approach, and section 4 presents the model results. Section 5 discusses the uncertainties in the approach, the implications for Europa and Ganymede, and possible extensions to this work.

### 2. Observations

[5] The surface of Europa is tectonically deformed and young, with a nominal surface age of 60 Myr [Zahnle *et al.*, 2003]. Bands (see Figure 1a) are a common class of tectonic features, identified as extensional on the basis of Voyager images [Schenk and McKinnon, 1989]. Bands are a few up to 30 km across, and consist of regions, often bounded by ridges, separating undeformed areas which were adjacent prior to band formation [Sullivan *et al.*, 1998; Tufts *et al.*,

<sup>1</sup>On leave at Department of Earth and Space Sciences, University of California, Los Angeles, California, USA.

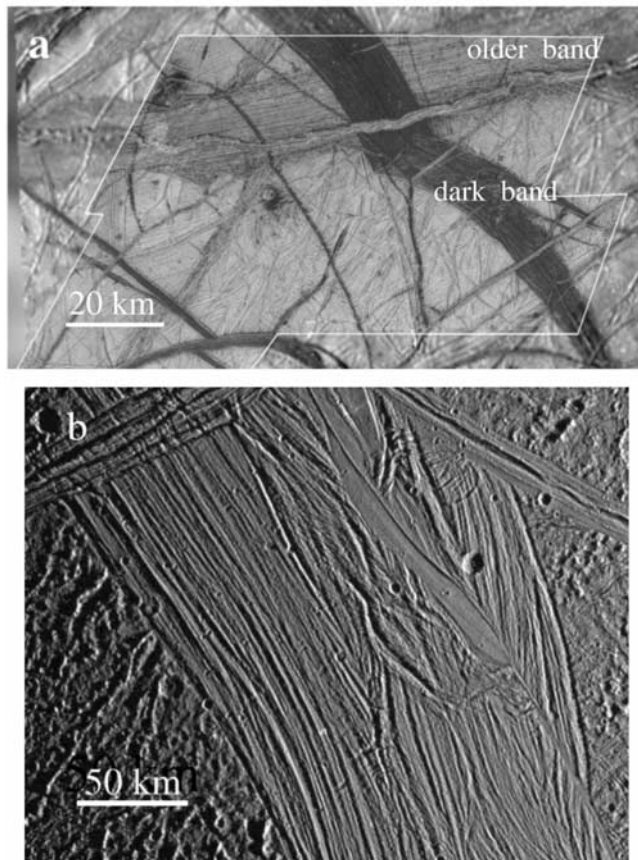


**Figure 1.** a) Typical band on Europa, modified from Figure 2 of *Prockter et al.* [2002]. Image resolution 55 m/pixel, from Galileo's twelfth orbit; north is up. Note that the dark NW-SE band cuts an earlier, less obvious ENE-WSW band. b) Typical grooved terrain on Ganymede, modified from PDS image (ID 394526201). Image from Galileo's eighth orbit, resolution 494 m/pixel, north is up. Image centered at 1°S, 204°E, taken at 14:15:07 UTC on 7th May 1997. The NW-SE trending groove lane is Tiamat Sulcus; the low sun angle emphasizes the rough topography.

2000; *Prockter et al.*, 2002]. Although bands are primarily extensional, there may also be a component of strike-slip motion [*Tufts et al.*, 2000]. Bands show subparallel lineaments, sometimes containing a medial valley and showing symmetry reminiscent of sea-floor spreading on Earth [*Sullivan et al.*, 1998; *Prockter et al.*, 2002]. Bands are sometimes elevated by  $\sim 100$  m with respect to their surroundings [*Prockter et al.*, 2002; *Nimmo et al.*, 2003b].

[6] Ganymede consists of two principal terrain types: dark terrain, which covers  $\approx 1/3$  of the surface and is nominally  $>4$  Gyr old [*Zahnle et al.*, 2003], and bright grooved terrain, 2–10 times less heavily cratered. Grooved terrain (see Figure 1b) is heavily deformed by crosscutting ridges and troughs, which are predominantly extensional in origin [*Parmentier et al.*, 1982; *Pappalardo et al.*, 1998]. Grooved lanes are typically hundreds of kilometers wide, and may extend along strike for several hundred kilometers. Some areas of ancient dark terrain also show evidence for tectonism similar to that observed in grooved terrain [*Patel et al.*, 1999]. There are local variations in faulting style

within the grooved terrain: high degrees of extension are typically accommodated by domino-style faulting, while lower degrees of extension result in horst-and-graben structures or simple fractures [*Pappalardo et al.*, 1998; *Collins et al.*, 1998a; *Patel et al.*, 1999]. The variations in extension may reflect a relatively complex, multi-stage origin of groove lanes [*Collins et al.*, 1998b]. Despite this complexity, on a broad scale extension on Ganymede appears to be typified by distributed deformation across relatively wide ( $\sim 100$  km) zones. However, there may also be a few Europa-like spreading centers. The best example is Arbelá Sulcus [*Head et al.*, 2002], although other examples may exist [*Collins et al.*, 2001].

[7] The stretching factor of a feature is defined as the ratio of its final to initial width. High resolution stereo images of Uruk Sulcus on Ganymede suggest that the domino-style faulting produces stretching factors of at least 1.51–1.58 [*Collins et al.*, 1998a]. Stretching factors are probably smaller in the less heavily faulted horst-and-graben areas. A study of strained craters in dark and bright terrains produced stretching factors across the entire crater of 1.03–1.49 and 1.14, respectively (R. T. Pappalardo and G. C. Collins, Strained craters on Ganymede, submitted to *Journal of Structural Geology*, 2003). The stretching factor of bands on Europa is more difficult to assess. Since the two edges of a band can be fit back together by removing the band entirely, the stretching factor is essentially infinite (the original band width was zero).

[8] There are few estimates of shell properties for Ganymede. [*Dombard and McKinnon*, 2001] modeled the observed groove lane topography ( $\approx 10$  km wavelength) with a necking-type extensional instability and obtained strain rates and thermal gradients in the range  $10^{-16}$ – $10^{-14}$   $s^{-1}$  and 20–40  $K km^{-1}$  for Uruk Sulcus and Nicholson Regio. [*Collins et al.*, 1998a] used an older rheology and obtained values of  $\sim 10^{-14}$   $s^{-1}$  and  $\sim 20$   $K km^{-1}$  for Uruk Sulcus. *Nimmo et al.* [2002] obtained thermal gradients of 30  $K km^{-1}$  from flexural studies of two grooved terrain areas on Ganymede. These thermal gradients, if correct, would result in conductive shell thicknesses of roughly 4–8 km at the time of groove formation. On the basis of an analysis of dominant length scales in grooved terrain, *Patel et al.* [1999] concluded that the depth to the brittle-ductile transition (BDT) at the time of faulting was  $\sim 1$ –3 km. This BDT depth is consistent with the inferred conductive shell thickness (see section 5.1).

[9] The nature of the ice shell on Europa is highly uncertain. Several independent lines of evidence suggest a shell thickness of  $\approx 20$  km [*Moore et al.*, 1998; *Schenk*, 2002; *Hussmann et al.*, 2002; *Turtle and Ivanov*, 2002; *Nimmo et al.*, 2003a] but it is possible that the shell is as thin as 2 km [*Hoppa et al.*, 1999; *Greenberg et al.*, 2000]. Similarly, estimates of BDT depth are highly variable. The BDT depth of interest is that applicable at the start of rifting (see section 5). *Pappalardo et al.* [1999] summarize various lines of geological evidence suggesting a BDT depth of 1–3 km. Estimates based on impact crater studies [*Moore et al.*, 1998; *Kadel et al.*, 2000; *Schenk*, 2002] give values of 3–11 km. The high strain rates associated with impact processes are likely to produce deeper BDT's than the lower rates associated with geological timescales [*Golombek and Banerdt*, 1990]. High resolution images of bands give a

lineament spacing of 0.4 km [Prockter *et al.*, 2002] and suggest a comparable BDT depth during rifting. Part of the uncertainty may stem from temporal or spatial variations in the shell properties; it is also possible that some features, such as double ridges, are formed in a manner which alters the local mechanical properties of the shell [Nimmo and Gaidos, 2002]. Here I will assume that the BDT depth is in the range 0.5–3 km, in agreement with the geological observations. The effect of a greater BDT depth is discussed in section 5.1. Finally, the strain rates on Europa responsible for the formation of bands are unknown.

[10] The approximate similarity of the syn-rift BDT depth on Ganymede to that for bands on Europa is in marked contrast to the different widths of the extensional features. Using Buck's [1991] classification, narrow rifts on Earth, such as the East African Rift, are those in which the BDT depth is comparable to the rift dimensions [e.g., Ebinger *et al.*, 1999], while wide rifts, such as the Basin and Range, have a width greatly exceeding the BDT depth [Hamilton, 1987]. By this analysis, the bands on Europa are examples of narrow rifts, while groove lanes on Ganymede are wide rifts.

[11] In summary, extension on Europa is accommodated by bands, zones of infinite extension (similar to mid-ocean ridges on Earth) which are 3–30 km wide. Extension on Ganymede, conversely, is accommodated by domino-style faulting across zones up to a few hundred kilometers wide, with lower stretching factors (up to 1.6 locally). In the next section, a model is described which will constrain the circumstances under which these two rifting modes are favored.

### 3. Model

#### 3.1. Overview

[12] The model described below is based on the approach of Buck [1991]. It also bears some resemblance to the analysis of Dombard and McKinnon [2001] but focuses on longer wavelength features than these authors. Before going into details, the main components of the model will be summarized. This model is simpler than more recent attempts to model terrestrial rifting [e.g., Christensen, 1992; Bassi, 1995; Davis and Kuszniir, 2002]. However, as will be discussed below, the relative paucity of data and the large uncertainties in the appropriate parameters to use (particularly the correct rheology) suggest that more sophisticated models are unlikely to yield further insights.

[13] When rifting occurs on a terrestrial continent, there are two main effects. Firstly, the crust and mantle are thinned. If the rifting is rapid relative to the rate at which heat can diffuse away, the vertically integrated strength of the lithosphere is reduced. However, if the rifting is slow relative to the diffusion timescale, the intrinsically stronger mantle will cool as it rises and may result in an increase in lithospheric strength. Thus the initial strain rate is an important parameter in determining the effects of extension [England, 1983; Kuszniir and Park, 1987; Newman and White, 1999].

[14] Secondly, as extension proceeds, lateral variations in crustal thickness will develop. These lateral variations set up buoyancy forces which oppose further extension [Buck, 1991; Davis and Kuszniir, 2002]. However, if the crust is sufficiently thick or hot, it may flow laterally in response to these buoyancy forces [e.g., Kruse *et al.*, 1991]. Lower

crustal flow reduces the forces opposing extension, and thus promotes further extension.

[15] Buck [1991] took both these effects into account in developing his model. His approach, followed here, was to specify a constant strain rate during extension, and to compare the forces present initially with those after a specified amount of extension had taken place. If the net force had decreased, then further extension in that area was favored (since it would take more force to cause extension elsewhere). This situation was inferred to lead to narrow rifting. If, however, the net force had increased, extension elsewhere would be favored, leading to wide rifting.

[16] Buck [1991] also identified two kinds of narrow rifting, one of which was associated with lower crustal flow and the development of metamorphic core complexes. Because of the paucity of data on icy satellites, this distinction is less important here. It will be assumed that if the net force decreases during extension, rifting will remain localized and will lead to narrow, high stretching factor features similar to the bands on Europa. Conversely, if the net force increases, rifting will be spread out over a broad region with lower stretching factors, and will lead to features similar to grooved terrain on Ganymede.

[17] Although the basic analysis of Buck [1991] is followed below, icy satellite extension differs in several important respects from extension on silicate planets. The most important difference is that there is no equivalent of the mantle. Thus, when an icy satellite shell is thinned, there is no possibility of a strong mantle-like layer increasing the overall strength of the shell. Hence, on icy satellites, extension always leads to a reduction in strength. Another difference, which will become apparent below, is that lateral flow of material tends to be more important on icy than on silicate bodies [Stevenson, 2000; Nimmo, 2003].

#### 3.2. Model Geometry

[18] Figure 2a shows the model geometry adopted. Extension is assumed to happen over an area of width  $X_e$ , where the horizontal rifting velocity  $u(x)$  is given by

$$u(x) = \begin{cases} u_{\max} & x \geq X_e/2 \\ u_{\max} \sin(\pi x/X_e) & |x| < X_e/2 \\ -u_{\max} & x \leq -X_e/2 \end{cases} \quad (1)$$

where  $x = 0$  at the center of symmetry and  $u_{\max}$  is defined by the strain rate  $\dot{\epsilon}$ , assumed constant

$$u_{\max} = \dot{\epsilon} X_e/2. \quad (2)$$

The width of the computational domain  $X_f$  is larger than  $X_e$ . In the absence of flow in the lower part of the shell, the continuity condition  $\partial u/\partial x + \partial v/\partial z = 0$  gives the vertical velocity  $v(z)$  at the center of the rift

$$v(z) = \frac{-\pi \dot{\epsilon}}{2} z \quad (3)$$

where  $z$  is depth measured vertically downward from the surface.

[19] Extension leads to thinning, but if lateral flow is important, then near-surface layers will be thinned by a larger factor than the shell as a whole. It is therefore

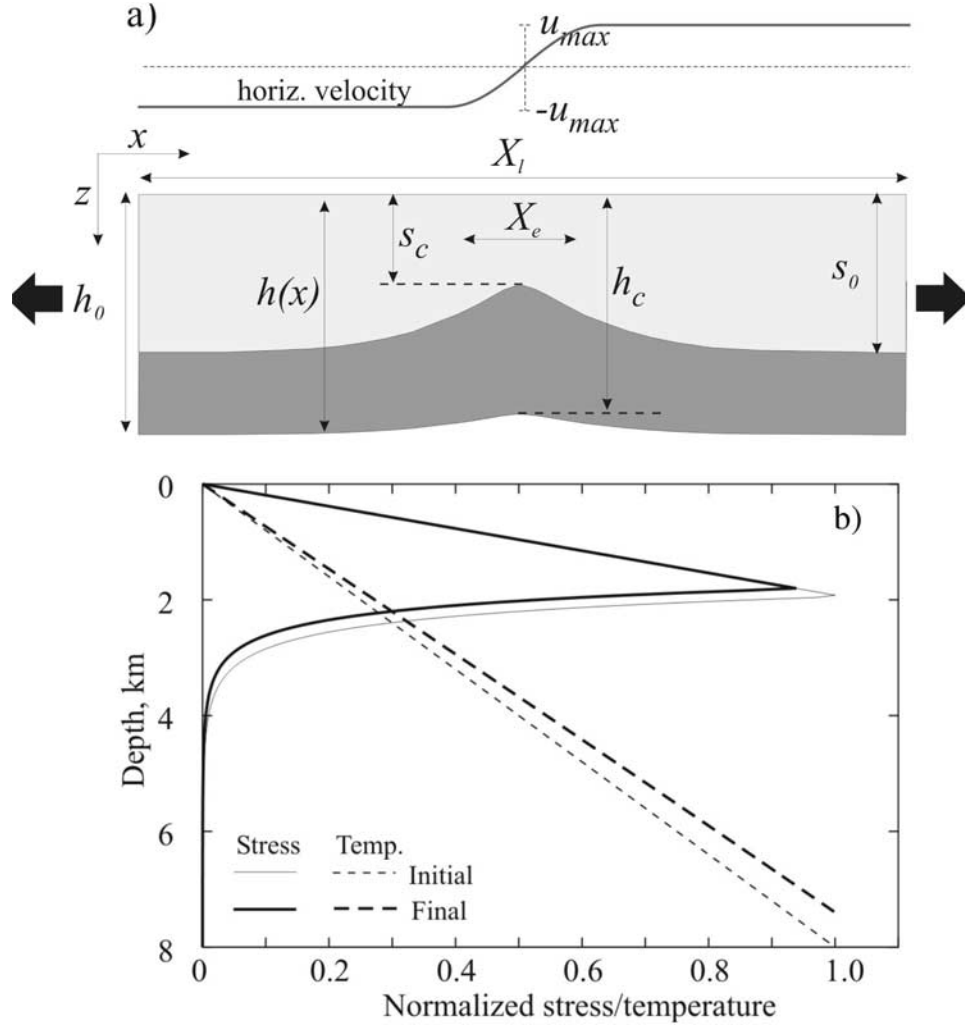


**Figure 2.** a) Definition sketch for geometry of model. Light gray and dark gray areas are parts of shell in which lateral flow is negligible and important, respectively. The extension factor for the shell as a whole is less than that for the near-surface layer because of lateral flow of ice. b) Normalized temperature and stress profiles at the center of the rift at the beginning and end of rifting. Temperature is normalized by the temperature at the base (260 K) and stress by the maximum initial stress (1.5 MPa). The final stretching factor  $\beta_{max}$  in this case was 1.37, but because of lateral shell flow the total shell thickness has only been reduced by a factor of 1.08. The temperature gradient has increased and the maximum stress decreased.  $\Delta F$  is  $0.28 \text{ GN m}^{-1}$ , indicating wide rifting will result. The strain rate was  $10^{-15} \text{ s}^{-1}$ , rifting duration 6.35 Myr and  $h_0$  8 km; other variables given in Table 1.

necessary to define two stretching factors, the total stretching factor  $\beta_t$  and the shallow stretching factor  $\beta_s$ , where

$$\beta_t = \frac{h_0}{h_c(t)} \quad \beta_s = \frac{s_0}{s_c(t)} \quad (4)$$

Here  $t$  is time, and  $h_0$  and  $h_c(t)$  are the initial and later shell thickness at the center of the rift, respectively. Similarly,  $s_0$  and  $s_c(t)$  are the initial and later depth to a shallow marker (see Figure 2a). The extension observed at the surface (e.g., from summing fault displacements) will give  $\beta_s$ .

[20] The rate of shell thinning is controlled by  $v$ , and it can be shown that

$$\frac{d\beta_s}{dt} = \frac{\pi \dot{\epsilon}}{2} \beta_s \quad (5)$$

for the horizontal velocity variation assumed. If lower shell flow is not important, then  $\beta_t = \beta_s$ . Equation (5) may be used to obtain  $\beta_s$  given  $\dot{\epsilon}$  and the duration of rifting.

### 3.3. Temperature Evolution

[21] To determine the response of the ice shell to extension, its thermal evolution with time needs to be calculated. Throughout this work it will be assumed that heat is transferred through the shell by conduction alone. While convection is a possibility [McKinnon, 1999], it will be shown in section 4.1 that it is not likely to occur for the range of shell thicknesses obtained. Thus the assumption of a conductive temperature profile may be justified a posteriori. Following [Buck, 1991], lateral conduction of heat is assumed to be negligible. The temperature evolu-

tion at the center of the rifting region ( $x = 0$ ) is thus given by

$$\frac{\partial T}{\partial t} = \kappa \frac{\partial^2 T}{\partial z^2} - v \frac{\partial T}{\partial z} + H \quad (6)$$

where  $t$  is time,  $T(z)$  is the temperature,  $\kappa$  is the thermal diffusivity and  $z$  is positive downward.  $H$  is the internal heat generation rate and  $v$  is the vertical velocity. Here the thermal diffusivity is assumed to be constant. In general,  $H$  is assumed to be zero (see section 4.1). The temperatures at the surface and at the base of the shell are fixed at  $T_s$  and  $T_b$ , respectively. A minor difference between icy satellites and terrestrial rifting is that in the former, the temperature at the base of the ice shell is fixed, while in the latter the Moho temperature can vary.

### 3.4. Flow in the Lower Shell

[22] Geological materials deform according to the following law

$$\dot{\epsilon} = A' \sigma^n \exp(-Q/RT) \quad (7)$$

where  $A' = Ag_s^{-p}$ ,  $A$ ,  $Q$ ,  $n$  and  $p$  are rheological constants,  $g_s$  is the grain size,  $\sigma$  is the differential stress,  $R$  is the gas constant and  $T$  is temperature. In situations such as rifting where lateral pressure gradients develop, warm parts of the ice shell may flow at a rate determined by equation (7).

[23] The time evolution of lateral variations in shell thickness  $h(x)$  may be obtained using equation (7) and the methods of *Buck* [1991] and *Nimmo and Stevenson* [2001]:

$$\frac{\partial h}{\partial t} = -\frac{d}{dx} \left[ A' C e^{-Q/RT_b} (\rho^* g)^n \left| \frac{\partial h}{\partial x} \right|^{n-1} \frac{\partial h}{\partial x} \right] - u \frac{\partial h}{\partial x} - h \frac{\partial u}{\partial x}. \quad (8)$$

Here  $g$  is the acceleration due to gravity and  $\rho^* = \rho_m - \rho_c$ , where  $\rho_c$  and  $\rho_m$  are the density of ice and water, respectively. Note that the definition of  $\rho^*$  agrees with *Nimmo and Stevenson* [2001] but differs by a factor of  $\rho_c/\rho_m$  from that of *Buck* [1991]. The first term on the right hand side gives the lateral flow of crust under non-Newtonian conditions [see *Nimmo and Stevenson*, 2001], where  $C$  is a numerical constant with dimensions of  $m^{2+n}$  which is proportional to the horizontal flux of material. The quantity  $C$  increases with increasing shell thickness; thus lateral flow is more rapid in thicker shells. The second term gives the lateral advection of crustal thickness, and the third term gives the thinning of the crust due to extension [see *Buck*, 1991]. Note that  $C$  varies in time but not in space. For  $n = 1$  (i.e., Newtonian rheology) equation (8) reduces to equation (7) of *Buck* [1991]. The advantage of the approach used here over that of *Buck* [1991] is that the stress driving the flow does not have to be calculated on the basis of some a priori specified distance. The disadvantages are that this approach makes the calculations slower, and when  $n \neq 1$  it is not possible to derive a simple analytical criterion for the rift mode boundaries (the Goetze number of *Buck* [1991]).

[24] Because lower crustal flow transports relatively hot lower crustal material into areas where the crust has thinned, it will affect the temperature structure. This effect is

neglected by *Buck* [1991] and is also neglected here; for the parameters used, it is unlikely to change the results significantly (see section 4.1).

### 3.5. Forces

[25] As noted above, the balance of forces present changes as rifting proceeds, and it is this balance which determines whether wide or narrow rifts will be favored. There are three forces of interest [*Buck*, 1991]. Firstly, there is the yield strength of the lithosphere, i.e., the vertically integrated stress required to cause the specified strain rate. Near the surface, the ice will be cold and deform by brittle failure. At greater depth, the material will deform in a viscous fashion. The integrated strength of the crust is thus given by

$$F_{yse} = \int_0^h \sigma(T, z, \dot{\epsilon}) dz \quad (9)$$

where  $\sigma(T, z, \dot{\epsilon})$  is given by the smaller of  $\sigma_b$  and  $\sigma_v$ , where

$$\sigma_b = gBz, \quad \sigma_v = \left( \frac{\dot{\epsilon}}{A'} \right)^{1/n} \exp(Q/nRT). \quad (10)$$

Here  $\sigma_b$  is the brittle stress,  $\sigma_v$  is the ductile stress (obtained from equation (7)) and  $B$  is a constant which depends on the density and coefficient of friction of ice. Figure 2b shows a typical yield-strength envelope (YSE). In the shallow crust where temperatures are low, the ice deforms in a brittle manner, while at greater depths ductile deformation occurs. The depth at which the transition between the two occurs is the BDT depth, and the area under the YSE is usually dominated by the brittle contribution. The behavior of the BDT on icy satellites has previously been investigated by *Golombek and Banerdt* [1990] and *Ruiz and Tejero* [2000].

[26] Because the depth to the BDT increases with increasing strain rate,  $F_{yse}$  increases with  $\dot{\epsilon}$ . As noted above, because of the absence of a mantle, thinning of the shell always results in a reduction in  $F_{yse}$ , i.e., weakening. Figure 2b also shows this effect: the thinning crust and consequent increase in temperature gradient leads to a reduction in BDT depth and thus in  $F_{yse}$  as rifting proceeds.

[27] As rifting proceeds, lateral shell thickness variations will give rise to buoyancy forces,  $F_b$ , where

$$F_b = g\rho^* \left( h - \frac{\Delta h}{2} \right) \Delta h \approx g\rho^*(\beta_t - 1)h^2 \quad (11)$$

where  $\Delta h = h_0 - h_c(t)$  is the lateral shell thickness contrast (the initial shell thickness is assumed not to vary laterally). This equation reduces to equation (12) of *Buck* [1991] when  $\Delta h \ll h$ . Clearly, if lateral flow occurs such that  $\Delta h$  is reduced, then  $F_b$  is reduced. Figure 2b shows that the contrast in shell thickness is only about 20% of that expected from equation (5) because of the effect of lateral flow.

[28] Finally, there are also thermal buoyancy forces,  $F_{tb}$ , arising from the lateral variation in temperature structure as rifting proceeds. This contribution is given by

$$F_{tb} = g\rho\alpha \int_0^h \delta T(z)z dz \quad (12)$$

where  $\delta T(z)$  is the difference between the temperature at the center of the rift and the background temperature, and  $\alpha$  is the volumetric thermal expansivity. It will be shown below that  $F_{tb}$  is small compared to the other forces, because for icy satellites there is no lithospheric mantle equivalent to serve as a source of thermal buoyancy.

[29] As noted above, it is the change in forces over the course of extension that is important. These changes will be denoted by  $\Delta F_{yse}$ ,  $\Delta F_b$  and  $\Delta F_{tb}$ , respectively, and the net change in force will be  $\Delta F$ .  $\Delta F_{yse}$  is always negative, and  $\Delta F_b$  will be positive or zero. A positive  $\Delta F$  is likely to result in wide rifting, a negative value in narrow rifting (section 3.1).

### 3.6. Numerical Procedure

[30] The initial conditions are that the shell thickness  $h(x)$  is a constant value  $h_0$  everywhere, and the initial temperature structure is found using the steady-state version of equation (6) with  $u = 0$ . At time  $t = 0$  rifting begins, by specifying a velocity gradient (equation (1)) across the central portion of the shell (see Figure 2a). Because of symmetry, only half the space shown in Figure 2a needs to be modeled. The temperature structure at the center of the rift is updated using a finite-difference version of equation (6). The diffusion term is updated using FTCS and the advective term with upwind differencing [Press *et al.*, 1992]. The vertical node spacing  $\Delta z$  is 0.005 of the initial shell thickness  $h_0$ . The number of nodes in the vertical direction is reduced as  $h$  decreases, but  $\Delta z$  is constant except for the deepest point. The temperature at the bottom node is fixed at  $T_b$  and  $v$  is calculated using equation (3). The time step  $\Delta t$  is kept at a constant value of  $10^{-7}/\dot{\epsilon}$  s unless it needs to be reduced due to rapid lateral flow (see below) or because the Courant criterion (set by the vertical length scale) has been exceeded.

[31] Given an updated temperature field  $T(z)$ , equation (8) is solved using FTCS for the diffusion and upwind differencing for the advective terms; more details are given by Nimmo and Stevenson [2001]. The boundary conditions are reflecting at  $x = 0$  and  $x = X/2$ , and the horizontal node interval  $\Delta x$  is set to 0.25 km.  $C$  is found by numerical integration and the requirement that the horizontal flow velocity is zero at the surface. If  $\Delta t$  results in a maximum change in  $h$  greater than 100 m over one iteration, the value of  $\Delta t$  is reduced. The model is terminated when the shallow extension factor  $\beta_s$  reaches a preset value  $\beta_{max}$ . If required, the subsequent relaxation of the shell thickness contrasts can be followed simply by setting  $u = 0$  and proceeding as above.

[32] For integer  $n$  analytical expressions for  $C$  (equation (8)) may be derived [e.g., Nimmo *et al.*, 2003b] and it was verified that the numerical solution gave the same results. The numerical solution was also checked by setting  $n = 1$  and imposing an initial shell thickness contrast, for which there is an analytical solution to equation (8) when  $u = 0$ . By setting  $T_b$  to an artificially cold value, lateral flow is suppressed and it was verified that the model stretching factors agreed with the analytical expression (equation (5)).

[33] The results were insensitive to reductions in  $\Delta t$  or  $\Delta x$ . Reducing  $\Delta z$  from 0.005  $h_0$  to 0.0025  $h_0$  resulted in a 6% change in  $\Delta F$ , with further reductions producing <1%

**Table 1.** Parameters Adopted<sup>a</sup>

Quantity	Value	Units
$T_s$	110	K
$X_e$	20	km
$k$	3.25	W m <sup>-1</sup> K <sup>-1</sup>
$\rho_c$	900	kg m <sup>-3</sup>
$g$	1.3	m s <sup>-2</sup>
$\beta_{max}$	1.08	-
$n$	1.8	-
$p$	1.4	-
$T_b$	260	K
$X_l$	100	km
$\alpha$	$1.2 \times 10^{-4}$	K <sup>-1</sup>
$\rho_m$	1000	kg m <sup>-3</sup>
$B$	600	kg m <sup>-3</sup>
$Q$	49	kJ mol <sup>-1</sup>
$A$	$6.2 \times 10^{-14}$	Pa <sup>-1.8</sup> m <sup>1.4</sup> s <sup>-1</sup>
$g_s$	1	mm

<sup>a</sup>Values of  $n$ ,  $Q$ ,  $A$ , and  $p$  are for rheology B; values for rheology A are given in the caption to Figure 4.

change. Given the other uncertainties involved, these changes are unlikely to affect the results.

### 3.7. Parameters Adopted

[34] The parameters adopted are summarized in Table 1; the effects of uncertainties in these parameters are discussed in section 4.1. Although some parameters are likely to vary slightly between Ganymede and Europa, one set of values is adopted here for simplicity. The surface temperature is assumed to be 110 K, approximately representative of values on Ganymede and Europa [Ojakangas and Stevenson, 1989; Dombard and McKinnon, 2001], and  $T_b$  is 260 K, to take into account the likely effect of pressure and/or salinity on the melting temperature of ice. Although the thermal conductivity  $k$  of ice varies as  $1/T$  [Klinger, 1980] it is assumed to be constant here. The value of  $k$  adopted gives the same heat flux as the  $T$ -dependent case for the values of  $T_b$  and  $T_s$  assumed here. The constant  $B$  is 600 kg m<sup>-3</sup>, implying a coefficient of friction of 0.67, in agreement with laboratory measurements [Beeman *et al.*, 1988]. The density of pure water ice at 260 K is 917 kg m<sup>-3</sup> [Kirk and Stevenson, 1987]; I have adopted a slightly lower value to take into account the possibility of near-surface porosity reducing the overall density [Nimmo *et al.*, 2003b].

[35] As will be seen below, the results are affected by choices of  $X_e$  and  $\beta_{max}$ . The width of the extending region  $X_e$  is chosen to be similar to typical band widths. The maximum amount of extension  $\beta_{max}$  is 1.08, similar to the smallest values observed for Ganymede grooved terrains. Since the main issue is whether or not extension localizes in one area as rifting proceeds, it is appropriate to use a low value of  $\beta_{max}$  to represent the early stages of rifting. The effect of varying  $\beta_{max}$  is discussed further in section 4.1.

[36] By far the largest uncertainty in these parameters is that of the rheology of water ice. Goldsby and Kohlstedt [2001] summarized ice rheologies for a range of stresses, temperatures and grain sizes. For the conditions of interest here, deformation is likely to be dominated by the whichever is the slower of: basal slip-accommodated grain boundary sliding (rheology A); and grain boundary sliding-accommodated basal slip (rheology B). For likely grain sizes, rheology B will be the rate-limiting mechanism and

will be adopted as the nominal rheology. The grain size of ice on Europa or Ganymede is unknown, but a nominal value of 1 mm will be used, similar to the 1–10 mm range observed in terrestrial sea ice [Budd and Jacka, 1989]. Although the experimentally-derived constants are sometimes corrected to account for the different model geometry [Ranalli, 1995; Dombard and McKinnon, 2001], this effect is very minor and is neglected here. A further complication is that, close to its melting temperature, the rheological behavior of ice changes [Goldsby and Kohlstedt, 2001], which means that lateral flow near the base of the ice shell may be enhanced. This effect is also neglected.

#### 4. Results

[37] Figure 3 plots  $\Delta F_b$ ,  $\Delta F_{yse}$  and  $\Delta F_{tb}$  as a function of initial shell thickness  $h_0$ . As noted above,  $\Delta F_{yse}$  is always negative. As the shell thickness increases, the depth to the BDT also increases and thus  $\Delta F_{yse}$  becomes more negative: shell weakening becomes more pronounced. The behavior of  $\Delta F_b$  is affected by lateral shell flow. In the absence of such flow, equation (11) shows that  $\Delta F_b$  should increase as  $h^2$ . The increase is actually more gradual than this, because lateral flow reduces the final shell thickness contrasts and thus the buoyancy forces.  $\Delta F_{tb}$  is a minor contribution compared to the other two, and is always negative. The net result of these three forces,  $\Delta F$ , is also shown in Figure 3. For this particular rheology and strain rate,  $\Delta F$  is positive at low shell thicknesses. Because  $\Delta F_{yse}$  changes more rapidly than  $\Delta F_b$ , the net force becomes negative beyond some critical value of  $h_0$  (15 km for  $\dot{\epsilon} = 10^{-15} \text{ s}^{-1}$ ). Thus, at low shell thicknesses, the wide rift mode is favored, while at large shell thicknesses, narrow rifts will occur. Other rheologies and strain rates produce broadly similar behavior (see below). Similar results for Earth were obtained by Buck [1991, Figures 8 and 9].

[38] Figure 4a shows the effect on  $\Delta F$  of shell thickness and strain rate. The main effect of varying  $\dot{\epsilon}$  is to alter the value of  $\Delta F_{yse}$  (equation (9)). An increased strain rate leads to larger BDT thicknesses and larger negative values of  $\Delta F_{yse}$ , that is, weakening is more effective. Thus the

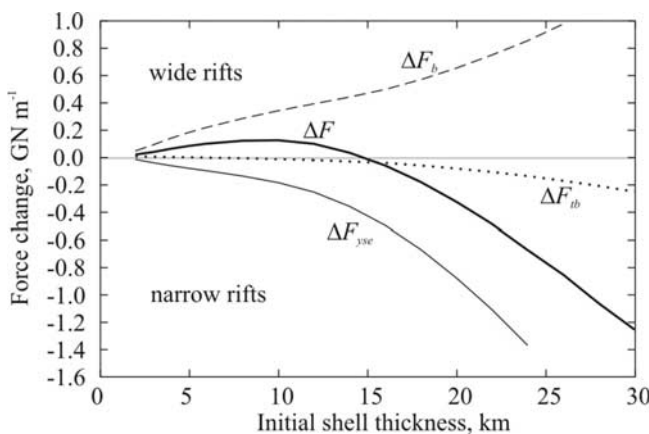


**Figure 3.** Variation in force changes during rifting as a function of initial shell thickness  $h_0$ . Strain rate  $10^{-15} \text{ s}^{-1}$ , other parameters given in Table 1. Positive  $\Delta F$  is likely to lead to wide rifts and negative  $\Delta F$  to narrow rifts (see text).

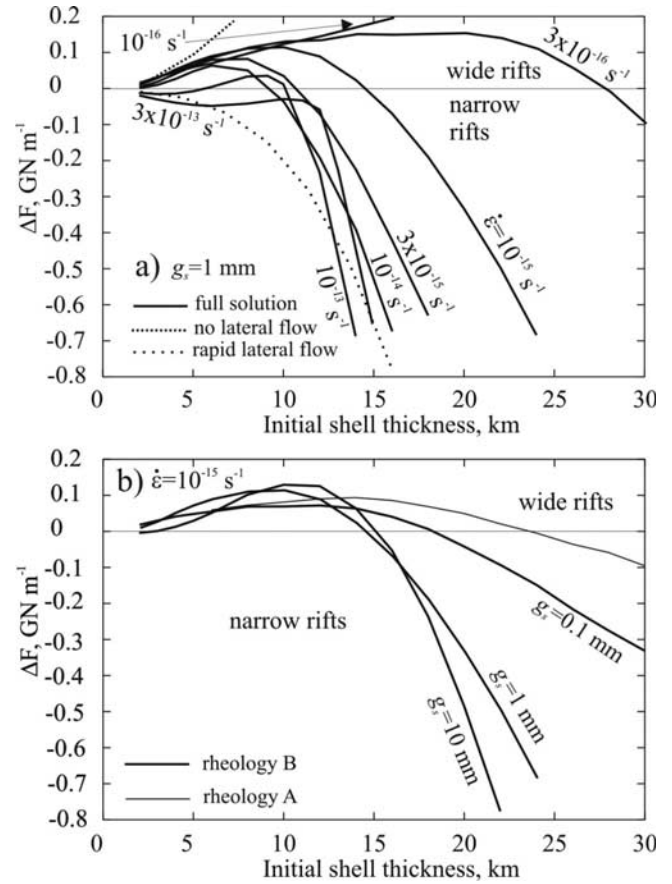


**Figure 4.** a) Variation in  $\Delta F$  with  $h_0$  and strain rate  $\dot{\epsilon}$  for rheology B. Wide dotted and narrow dotted lines are calculations with  $\dot{\epsilon} = 10^{-15} \text{ s}^{-1}$  for the case in which lateral shell flow is instantaneous and does not occur, respectively. b) Effect on  $\Delta F$  of varying rheology when  $\dot{\epsilon} = 10^{-15} \text{ s}^{-1}$ . Bold lines use rheology B with grain size specified; thin line is for rheology A for which  $n = 2.4$ ,  $Q = 60 \text{ kJ mol}^{-1}$  and  $A = 2.2 \times 10^{-7} \text{ Pa}^{-2.4} \text{ s}^{-1}$ .

transition to the narrow mode of rifting occurs at lower values of  $h_0$  as strain rate increases. At sufficiently high strain rates ( $> 2 \times 10^{-13} \text{ s}^{-1}$ ), narrow rifting is favored for all shell thicknesses. Conversely, for low strain rates ( $\leq 10^{-16} \text{ s}^{-1}$ ),  $\Delta F$  never becomes negative and the wide rifting mode is favored at all shell thicknesses. At low shell thicknesses, the competition between shell weakening and buoyancy forces can result in either narrow or wide rifts, depending on the strain rate.

[39] Figure 4a also shows end-member cases for  $\dot{\epsilon} = 10^{-15} \text{ s}^{-1}$ . In one case (wide dotted line), lateral flow is assumed to happen instantaneously so that  $\Delta h = 0$  throughout, and thus  $\Delta F_b = 0$ . In this case,  $\Delta F$  is always negative and is similar to the behavior of the full solution at large shell thicknesses, when lateral flow is rapid. In the other case (narrow dotted line), lateral flow does not occur at all, so that  $\beta_t = \beta_s$ . In this case,  $\Delta F$  increases rapidly, and is similar to the behavior of the full solution at small shell thicknesses, when lateral flow is slow.

[40] Figure 4b shows the effects of varying the rheology and grain size. The bold lines use rheology B with varying

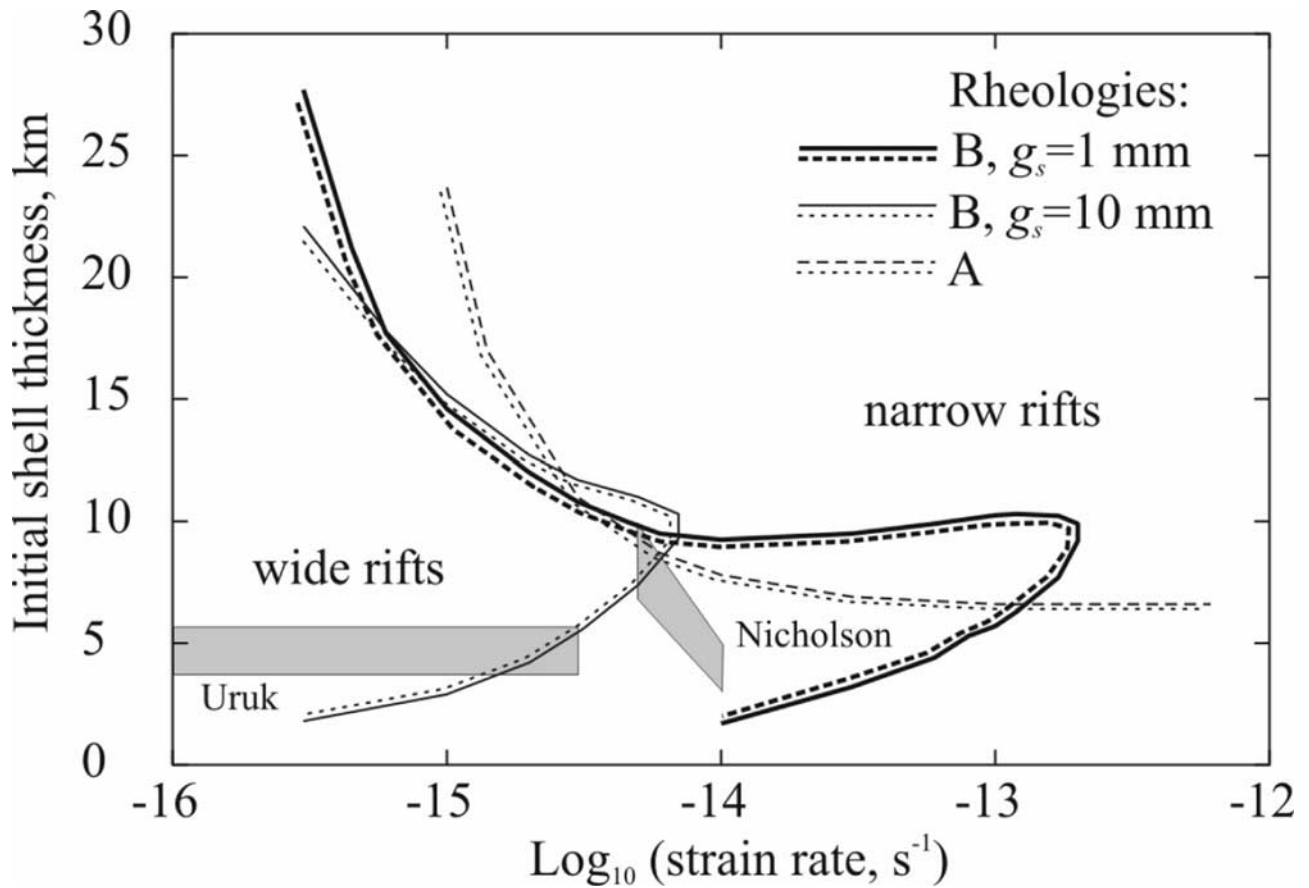


**Figure 5.** Mode transition between wide (+ve  $\Delta F$ ) and narrow (–ve  $\Delta F$ ) rifts as a function of strain rate and initial shell thickness. Dashed side of line indicates area where wide rifts are favored. Solid lines are for rheology B with grain size ( $g_s$ ) specified; dashed line is for rheology A. Light gray boxes are results from *Dombard and McKinnon* [2001] for two regions (Uruk Sulcus and Nicholson Regio) of Ganymede. Uncertainty is mainly due to the range of grain sizes assumed by these authors. See text for further discussion of this figure.

grain sizes and the thin line uses rheology A. Although the overall behavior of these different rheologies is similar to the nominal result, in detail they are different. For rheology A the depth to the BDT is shallower than in the nominal case, resulting in a smaller value of  $|\Delta F_{yse}|$  which displaces the curve upward at large shell thickness. The behavior of rheology B is similar when  $g_s = 0.1$  mm. When  $g_s = 10$  mm,  $\Delta F$  starts slightly negative, increases to a positive value as shell thickness increases, and then becomes negative again at even higher values of  $h_0$ . Thus, in this case narrow rifting is favored at very low or high shell thicknesses, while at intermediate thicknesses wide rifting is preferred. This behavior is similar to that for  $\dot{\epsilon} = 10^{-13} \text{ s}^{-1}$  in Figure 4a.

[41] Figure 4 shows that rifting behavior is likely to depend on shell thickness, strain rate and rheology. Figure 5 summarizes the results of Figure 4 and shows the mode transitions from wide to narrow rifting as a function of  $h_0$  and  $\dot{\epsilon}$ . High strain rates favor narrow rifts, because the BDT depth is greater and thus shell weakening is more pronounced. High shell thicknesses also favor narrow rifts, because lower shell flow is rapid and thus buoyancy forces are reduced. For the nominal rheology, narrow rifting may also occur at low shell thicknesses ( $h_0 < 10$  km), with the transition moving to smaller values of  $h_0$  as

strain rate decreases. At very high strain rates ( $> 2 \times 10^{-13} \text{ s}^{-1}$ ),  $\Delta F$  is never positive (see Figure 4a) and narrow rifting is thus favored at all shell thicknesses.

[42] An increase in grain size leads to more pronounced weakening, and thus allows narrow rifts to occur at lower strain rates. The behavior is otherwise similar to that for the nominal grain size. However, for rheology A narrow rifting is only favored at relatively high shell thicknesses ( $h_0 > 7$  km) and high strain rates. The behavior of rheology B when  $g_s = 0.1$  mm (not shown) is similar. A common result of all these rheologies is that narrow rifts are favored at high strain rates or large shell thicknesses. The behavior at low shell thicknesses ( $< 10$  km) is less predictable and depends on the rheology assumed.

#### 4.1. Sensitivity Analysis

[43] The above results are based on a particular set of parameters (Table 1), some of which are poorly known, so it is important to investigate the sensitivity of the results to variations in these parameters. Below, I discuss the effects of varying parameters on the curve shown in Figure 4a for which  $\dot{\epsilon} = 10^{-15} \text{ s}^{-1}$ . For the nominal parameters, rifting changes from wide to narrow at a critical shell thickness of 15 km.

[44] The factors influencing the brittle behavior of ice are relatively well known and do not significantly affect the results shown in Figure 4a. Altering  $B$  or  $g$  by 10% has negligible effect on the results. Increasing  $\rho_c$  by  $20 \text{ kg m}^{-3}$  results in a reduction in the critical value of  $h_0$  by 2 km, because  $\Delta F_b$  is reduced (equation (11)).

[45] Doubling  $X_l$  to 200 km results in minor (<10%) changes to the results. Such a small effect is to be expected if the boundaries of the domain have not experienced significant lateral flow. Changing  $X_e$ , on the other hand, has a significant effect because the rapidity of lateral shell flow is strongly wavelength dependent [Stevenson, 2000; Nimmo, 2003]. Reducing  $X_e$  to 10 km changes the critical shell thickness from 15 km to 11 km, since lateral flow is more rapid over shorter distances. It is not clear what value of  $X_e$  to use, although the observed band width probably gives an upper bound. If the initial rifting scale is controlled by the shell thickness, as seems likely, then a value of  $X_e$  comparable to  $h_0$  is appropriate. A reduction in  $X_e$  moves the curves in Figure 5 to lower strain rates, expanding the parameter space in which narrow rifting is favored. This result is most important for Europa: it would reduce the strain rate required, but have little effect on the inferred shell thickness (see section 5.1).

[46] Increasing  $\beta_{\max}$  to 1.17 and 1.37 results in the critical value of  $h_0$  increasing to 17 km and 24 km, respectively. Although lateral flow has longer to remove shell thickness contrasts, the increased magnitude of these contrasts increase  $\Delta F_b$  and move the curves of Figure 4a upward. The use of a stretching factor similar to grooved terrain values (see section 2) is probably appropriate, since wide and narrow rifts should exhibit different behavior even at low stretching factors [Buck, 1991].

[47] The thermal structure of the ice shell is poorly known and can have large effects on the results. Adding  $1 \mu\text{W m}^{-3}$  internal heating (equivalent to  $10 \text{ mW m}^{-2}$  surface heat flux increase when  $h_0 = 10 \text{ km}$ ) increases the critical thickness by 4 km because the increased temperature of the near-surface reduces the depth of the BDT. Unfortunately, the amount of internal heating within icy satellite shells is very poorly constrained (though see Hussmann *et al.* [2002]) so that it is hard to assess the importance of this parameter. Increasing  $T_b$  to 270 K does not affect the curves significantly. Altering  $T_s$  has a significant effect on the behavior of Figure 4, because it alters the BDT depth. Reducing  $T_s$  to 100 K results in the critical shell thickness reducing to 12.5 km, because the effect of  $\Delta F_{yse}$  is enhanced. The relatively large change is a result of the sensitivity of ice viscosity to temperature changes (equation (7)), and is discussed further below.

[48] As noted by Buck [1991], a problem with the model is that the thermal and material flow equations are not fully coupled, because the temperature evolution (equation (6)) does not take into account the velocity perturbation imposed by the lateral flow (equation (8)). Fortunately, this effect is likely to be small because the effective channel thickness in which lateral flow is important is only about 5% of the total shell thickness [Nimmo, 2003]. Modifying the vertical velocity (equation (3)) so that it is reduced toward the base of the crust (where lateral flow is important) affects the critical shell thickness by <1 km.

[49] The model assumes that the temperature profile is controlled by conductive processes and that convection does

not occur. For the range of shell thicknesses applicable to Ganymede and Europa (see below), this assumption is reasonable. Using the parameters in Table 1 and the time-dependent, non-Newtonian parameterization of *Solomatov and Moresi* [2000], the minimum shell thickness required to initiate convection is 52 km for rheology A. For rheology B, the minimum shell thickness is 55 km when the grain size is 0.1 mm (and correspondingly larger for larger grain sizes). Tidal dissipation could reduce this minimum shell thickness, but would need to exceed  $O(10^{11})W$  to do so. Such dissipation rates are possible, but by no means assured [Hussmann *et al.*, 2002].

[50] In summary, likely uncertainties may move the curves of Figure 4a up or down, and produce corresponding changes in the critical shell thickness of  $\approx \pm 5 \text{ km}$ . The most important uncertainties are those relating to the rheology of the ice shell, and its thermal structure (especially the degree of internal heating). However, the overall shape of the curves is not significantly affected.

## 5. Discussion

### 5.1. Application to Europa and Ganymede

[51] Figure 5 shows the principal result of this paper, namely that narrow rifts are favored for high strain rates or high shell thicknesses, while wide rifts are generally favored at low strain rates. Section 2 showed that extension on Europa typically results in narrow rifts, while rifts on Ganymede are wide. Figure 5 can therefore be used to place constraints on conditions on these two bodies at the time that rifting was occurring.

[52] For Ganymede the results are complicated by the fact that rifting happened early in its history, possibly during an episode of high transient eccentricity [Showman and Malhotra, 1997], and the shell conditions then are unlikely to resemble the present-day shell conditions. However, Figure 5 shows that it is actually quite difficult to generate wide rifts. For rheology B, shell thicknesses  $>10 \text{ km}$  only produce wide rifts at relatively low strain rates (less than  $\approx 3 \times 10^{-15} \text{ s}^{-1}$ ). For rheology A, a shell thickness of  $<7 \text{ km}$  at the time of rifting is required at high strain rates, though this condition becomes less restrictive at lower strain rates.

[53] The results of *Dombard and McKinnon* [2001] may be used as an additional constraint for Ganymede. The values of  $dT/dz$  and  $\dot{\epsilon}$  obtained by these authors are the best estimates currently available for Ganymede grooved terrain, and are plotted in Figure 5. Here  $dT/dz$  has been converted to shell thickness  $h_0$  by assuming no internal heating, top and bottom temperatures of 110 K and 260 K, respectively, and an uncertainty in the thermal gradient of  $\pm 20\%$ . The range in  $\dot{\epsilon}$  is due to the range of grain sizes assumed. The inferred values of  $h_0$  and  $\dot{\epsilon}$  are consistent with the observed wide rifts on Ganymede, except possibly for Nicholson Sulcus when  $g_s = 10 \text{ mm}$ . This agreement suggests that the model used here is appropriate.

[54] The mean surface age of Europa is  $\approx 60 \text{ Myr}$  [Zahnle *et al.*, 2003]. In this time, a conductive ice shell which was not internally heated could solidify to  $\approx 65 \text{ km}$  thickness [Turcotte and Schubert, 1982]. However, as noted in section 2, the present-day shell thickness on Europa is uncertain by at least an order of magnitude. Figure 5 shows

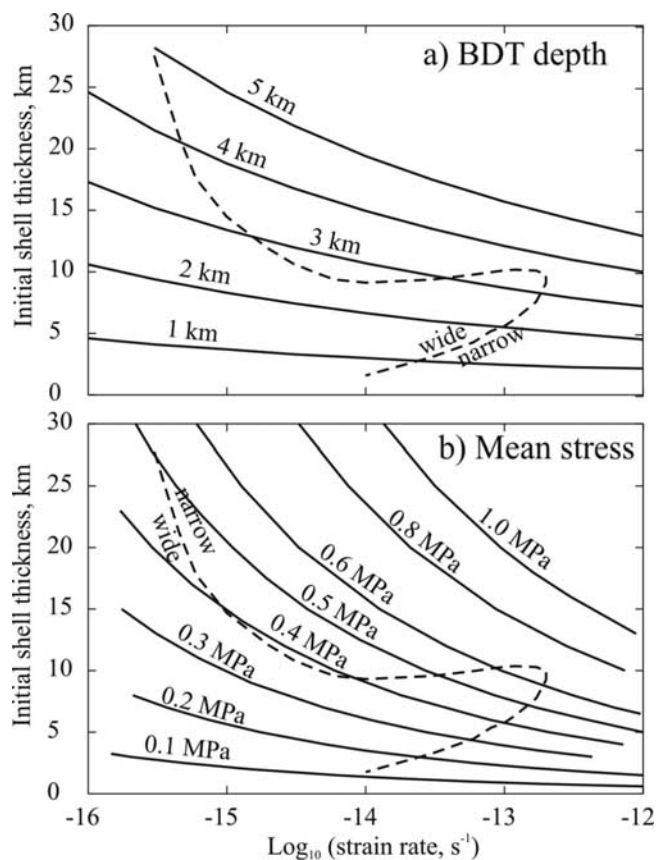


**Figure 6.** a) Depth to brittle-ductile transition (BDT) as a function of shell thickness and strain rate, calculated using method described in section 3.5. Dashed lines are rift transition for nominal rheology re-plotted from Figure 5. b) Mean stress required to cause a given strain rate as a function of shell thickness (see text). Dashed lines as for Figure 6a.

that for a shell thickness of 20 km, narrow rifting (as observed) is only possible if strain rates exceeded  $0.5\text{--}1 \times 10^{-15} \text{ s}^{-1}$ . Larger shell thicknesses would reduce these minimum strain rates. For a 2 km shell thickness, narrow rifting is only possible with the nominal rheology at high strain rates ( $>10^{-14} \text{ s}^{-1}$ ), and is not possible at all for rheology A. Whether a thick shell or a thin shell scenario is more likely is discussed further below.

[55] An additional constraint for both Ganymede and Europa may be obtained using the inferred depth to the BDT (see section 2). Figure 6a plots the BDT depth obtained using the methods of section 3.5 for the nominal rheology, and shows that the depth is relatively insensitive to large variations in strain rate. The results of *Dombard and McKinnon* [2001] for Ganymede suggest a BDT thickness of 1–2 km, consistent with the observations.

[56] The results for Europa are more difficult to assess. The most likely prerift BDT depth for Europa appears to be 0.5–3 km, though there are considerable uncertainties in this value (see section 2). Figure 6a shows that there are two regions in which both the BDT depth and the requirement for narrow rifting can be satisfied. Either the shell is thin ( $<8$  km) and the strain rate high ( $>10^{-14} \text{ s}^{-1}$ ), or the shell is

thicker (9–13 km) and the strain rate lower ( $0.15\text{--}3 \times 10^{-14} \text{ s}^{-1}$ ). Using a larger grain size produces similar constraints on shell thickness but reduces the minimum strain rate. For rheology A, shell thicknesses would need to be in the range 7–12 km. Taking into account the rheological and other uncertainties, the constraints of narrow rifting and BDT depth require a strain rate  $>10^{-15} \text{ s}^{-1}$  and a shell thickness  $<15$  km. Although thicker shells can also produce narrow rifts, they result in BDT depths greater than 3 km. If the BDT depth is actually greater than 3 km, larger shell thicknesses become acceptable.

[57] On the basis of Figures 5 and 6a, there are two possible explanations for the difference in rifting modes on Ganymede and Europa. Firstly, the shell thicknesses could have been comparable ( $\approx 4$  km), but strain rates on Ganymede were significantly lower than those on Europa (e.g.,  $10^{-14} \text{ s}^{-1}$  vs.  $10^{-13} \text{ s}^{-1}$ , respectively). Alternatively, the strain rates could both have been  $\approx 10^{-14} \text{ s}^{-1}$ , but shell thicknesses on Ganymede were lower than those on Europa (e.g., 4 km and 12 km, respectively). Which of these two alternatives is correct is unclear, and depends mainly on the highly uncertain BDT depth prior to rifting on Europa. The first option produces a shallower BDT depth than the second.

[58] The likelihood of the results can be checked by considering the stresses required to cause the inferred strain rates. At the start of rifting, the total force required to cause rifting is  $F_{yse}$ , and the mean (vertically averaged) stress is simply  $F_{yse}/h_0$ . Figure 6b plots the mean stress as a function of strain rate and shell thickness. Increasing strain rate requires an increase in mean stress, as expected, and increased shell thicknesses require higher stresses to produce the same strain rate. The *Dombard and McKinnon* [2001] Ganymede strain rates and shell thicknesses are compatible with a mean stress of 0.1–0.3 MPa, while the Europa results could be explained by a mean stress of 0.2–0.5 MPa. *Nimmo et al.* [2002] estimated stresses in the range 0.2–1.0 MPa from flexural studies of Ganymede grooved terrain, consistent with the values obtained here. Similarly, the stress level for Europa obtained here is similar to or slightly smaller than that inferred from flexural studies of one European feature [*Nimmo et al.*, 2003a]. Since these stresses are relevant to the period of rifting, they do not necessarily give the present-day stresses.

[59] Figure 6b shows that relatively small variations in mean stress can lead to a change in rifting mode. This phenomenon may provide an explanation for the observation that Ganymede apparently exhibits narrow rifting in places (see section 2), even though wide rifting is more common. Similarly, if the stress level on Ganymede stayed the same as its ice shell thickened, the strain rate would have dropped rapidly and a transition from narrow to wide rifting could have occurred (Figure 6b). Determining the relative ages of narrow and wide rifting episodes on Ganymede by geological mapping would provide a useful test of this hypothesis.

[60] A potentially important result of this analysis is that the BDT depth and narrow rifting criteria can best be satisfied for Europa by a relatively thin shell ( $<15$  km). Since it is the inferred BDT depth which provides the strongest constraint on shell thickness, it is of great importance to obtain better estimates of this poorly-known quan-

ity. Furthermore, it is not clear that a thin shell is required at the present day. Although bands appear to form at various points in the stratigraphic column, they generally predate lenticulae [Prockter *et al.*, 2002], and may thus be relatively old features. On the other hand, if bands are recent features, this study implies a relatively low present-day shell thickness. Accordingly, establishing where bands lie in the stratigraphic column should be a high priority of future geological mapping.

[61] The inferred strain rate for Europa of  $>10^{-15} \text{ s}^{-1}$  implies that it will take  $<2$  Myr to accumulate 5% strain. The negative  $\Delta F$  associated with narrow rifting suggests that the strain rate will accelerate with time [Hopper and Buck, 1993], and thus that the total duration of an individual band formation event is unlikely to exceed 10 Myr. Since this timescale is considerably shorter than the nominal surface age of the satellite, systematic variations in crater density across individual bands should not be observed.

[62] A surprising result of section 4.1 is the effect that quite small changes in  $T_s$  have on the critical shell thickness. Thus, it is possible that rifting behavior on a single satellite could vary with latitude. Similarly, different rifting behavior on different satellites could potentially be explained simply by variations in  $T_s$ . However, since Ganymede at the time of rifting was probably colder than Europa [Dombard and McKinnon, 2001], this mechanism would predict narrow rifting on Ganymede and wide rifting on Europa, opposite to what is observed.

## 5.2. Applications Elsewhere

[63] Ganymede and Europa are not the only icy satellites which show signs of extension. Rifts have also been studied on Enceladus [Kargel and Pozio, 1996] and Miranda [Pappalardo *et al.*, 1997], and also occur on Ariel, Titania and Tethys [Cruikshank and Brown, 1986]. Most of these rifts appear to be wide relative to the likely BDT depth, with the possible exception of Miranda. The paucity of data makes any quantitative interpretation premature. However, the lower surface temperature on these satellites will favor narrow rifting over wide rifting (see above). At the same time, shell thicknesses are likely to be greater, owing to the rapid cooling of small bodies. Figure 5 therefore suggests that strain rates on these bodies are likely to be significantly lower than on the Galilean satellites. If the surface of Titan shows evidence of extension, analyses of the kind presented here should help to constrain that satellite's shell structure and dynamics.

## 5.3. Future Work

[64] As discussed in section 3, the model adopted here makes a number of simplifying assumptions. Although the limited amount of data available may not justify more complicated models, possible further work is discussed below.

[65] One important assumption is that the strain rate is constant during rifting. Since the model is terminated before rifting has proceeded very far ( $\beta_{\text{max}} = 1.08$ ) this assumption is reasonable. An alternative approach, which has been adopted by other authors [e.g., Hopper and Buck, 1993; Newman and White, 1999], is to assume that the remote force is constant, and calculate the resulting changes in strain rate with time. Since there is no information on strain

rate variations for the Galilean satellites, the analysis adopted here is probably more useful, since it predicts the (observable) rift morphology.

[66] The model presented here specifies the location of rifting at an arbitrary point. In reality, rifting is likely to occur where the ice shell is locally weakened. One likely possibility, motivated by the observation that bands on Europa often initiate at double ridges [Prockter *et al.*, 2002], is that double ridges are sites of shear-heating [Nimmo and Gaidos, 2002] and are thus weaker than the surroundings. Since shear heating requires a component of strike-slip motion, the observation that some bands on Europa also involve shear [Tufts *et al.*, 2000] may not be surprising. A thorough geological investigation of the links between bands and ridges would be useful.

[67] The source of the stresses responsible for extension on Ganymede and Europa is uncertain. A mean stress of 0.2–0.5 MPa is larger than the current diurnal tidal contribution on Europa [Greenberg *et al.*, 1998] but is comparable to that expected for non-synchronous rotation [Leith and McKinnon, 1996]. Variations in shell thickness elsewhere on the satellites, such as the melt-through events proposed by O'Brien *et al.* [2002], would produce comparable remote stresses. The sensitivity of the results to the mean stress (Figure 6b) suggests that lateral variations in stress may result in different rift behavior. Thus, if stress variations are simply related to the satellite coordinate system (as is the case for tides), there should be a correlation of rift style with position.

[68] A consequence of extension is subsidence [McKenzie, 1978]. As Figure 2a illustrates, the effect of lateral shell flow is to reduce lateral shell thickness contrasts, and hence the amount of subsidence observed. The timescale over which this flow occurs depends on the shell thickness and rheology; for the nominal rheology and 100 km wavelength features it is  $\sim 1$ –100 Myr for shell thicknesses of 10 km [Nimmo, 2003]. Some rifted areas on Ganymede do appear to be lower than their surroundings [Schenk *et al.*, 2001; Head *et al.*, 2002]. Since the present-day shell thickness on Ganymede greatly exceeds 10 km, the negative topography is unlikely to be due simply to slow lateral flow. An alternative explanation for the negative topography is lateral variations in shell density [Nimmo *et al.*, 2003b].

[69] The rate of lateral flow depends very strongly on shell thickness. If subsidence associated with rifting were identified on Europa, the timescale over which this subsidence could be maintained would depend on the shell thickness. Thus finding the age of band activity on Europa would provide an additional constraint on shell thickness.

## 6. Conclusions

[70] The key conclusions of this paper are shown in Figure 5: narrow rifting is favored at large shell thicknesses or high strain rates, and wide rifting at low strain rates. Together with the inferred BDT depth, Figure 5 can be used to obtain shell thicknesses and strain rates during rifting.

[71] For Ganymede, the shell thicknesses ( $\approx 4$  km) and strain rates ( $<10^{-14} \text{ s}^{-1}$ ) inferred by Dombard and McKinnon [2001] are consistent with the observed wide rifting and BDT depth. For Europa, a BDT depth of 0.5–3 km and narrow rifting can only be obtained at relatively

low shell thicknesses (<15 km) and high strain rates ( $>10^{-15} \text{ s}^{-1}$ ) at the time of rifting. Higher shell thicknesses can also produce narrow rifts, but would result in larger BDT depths. It is not clear whether this shell thickness applies to present-day Europa: accordingly, it is important to establish the age of band formation.

[72] The difference between rifting behavior on Ganymede and Europa is due to either higher strain rates or higher shell thicknesses on Europa at the time of rifting. These differences imply small differences in the mean stress level:  $\approx 0.2 \text{ MPa}$  for Ganymede and  $\approx 0.3 \text{ MPa}$  for Europa. These values are comparable with other estimates of stress levels based on flexural features.

[73] **Acknowledgments.** I am grateful to Bob Pappalardo for helpful discussions and Geoff Collins and Andrew Dombard for prompt, thorough, and constructive reviews. This work was supported by the Royal Society.

## References

- Bassi, G. (1995), Relative importance of strain rate and rheology for the mode of continental extension, *Geophys. J. Int.*, *122*, 195–210.
- Beeman, M., W. B. Durham, and S. H. Kirby (1988), Friction of ice, *J. Geophys. Res.*, *93*, 7625–7633.
- Buck, W. R. (1991), Modes of continental lithospheric extension, *J. Geophys. Res.*, *96*(B12), 20,161–20,178.
- Budd, W. F., and T. H. Jacka (1989), A review of ice rheology for ice-sheet modeling, *Cold Reg. Sci. Technol.*, *16*(2), 107–144.
- Christensen, U. R. (1992), An Eulerian technique for thermomechanical modeling of lithospheric extension, *J. Geophys. Res.*, *97*(B2), 2015–2036.
- Collins, G. C., J. W. Head, and R. T. Pappalardo (1998a), The role of extensional instability in creating Ganymede grooved terrain: Insights from Galileo high-resolution stereo imaging, *Geophys. Res. Lett.*, *25*(3), 233–236.
- Collins, G. C., J. W. Head, and R. T. Pappalardo (1998b), Formation of Ganymede grooved terrain by sequential extensional episodes: Implications of Galileo observations for regional stratigraphy, *Icarus*, *135*(1), 345–359.
- Collins, G. C., J. W. Head, R. T. Pappalardo, B. Nixon, B. Giese, and R. Wagner (2001), The formation of Arbelia Sulcus and other smooth linear features on Ganymede: Possible crustal spreading and shear, *Lunar Planet. Sci.*, *XXXII*, abstract 1498.
- Cruikshank, D. P., and R. H. Brown (1986), Satellites of Uranus and Neptune, and the Pluto-Charon system, in *Satellites*, edited by J. Burns and M. Matthews, pp. 836–873, Univ. of Ariz. Press, Tucson.
- Davis, M., and N. Kuznir (2002), Are buoyancy forces important during the formation of rifted margins?, *Geophys. J. Int.*, *149*, 524–533.
- Dombard, A. J., and W. B. McKinnon (2001), Formation of grooved terrain on Ganymede: Extensional instability mediated by cold, superplastic creep, *Icarus*, *154*, 321–336.
- Ebinger, C. J., J. A. Jackson, A. N. Foster, and N. J. Hayward (1999), Extensional basin geometry and the elastic lithosphere, *Philos. Trans. R. Soc. London, Ser. A*, *357*(1753), 741–762.
- England, P. C. (1983), Constraints on extension of continental lithosphere, *J. Geophys. Res.*, *88*, 1145–1152.
- Goldsby, D. L., and D. L. Kohlstedt (2001), Superplastic deformation of ice: Experimental observations, *J. Geophys. Res.*, *106*(B6), 11,017–11,030.
- Golombek, M. P., and W. B. Banerdt (1990), Constraints on the subsurface structure of Europa, *Icarus*, *83*, 441–452.
- Greenberg, R., et al. (1998), Tectonic processes on Europa: Tidal stresses, mechanical response and visible features, *Icarus*, *135*, 64–78.
- Greenberg, R., P. Geissler, B. R. Tufts, and G. V. Hoppa (2000), Habitability of Europa's crust: The role of tidal-tectonic processes, *J. Geophys. Res.*, *105*, 17,551–17,562.
- Hamilton, W. (1987), Crustal extension in the Basin and Range Province, southwestern United States, in *Continental Extensional Tectonics*, edited by M. P. Coward, J. F. Dewey, and P. L. Hancock, *Geol. Soc. Spec. Publ.*, *28*, 155–176.
- Head, J., et al. (2002), Evidence for Europa-like tectonic resurfacing styles on Ganymede, *Geophys. Res. Lett.*, *29*(24), 2151, doi:10.1029/2002GL015961.
- Helfenstein, P., and E. M. Parmentier (1983), Patterns of fracture and tidal stresses on Europa, *Icarus*, *53*, 415–430.
- Helfenstein, P., and E. M. Parmentier (1985), Patterns of fracture and tidal stresses due to non-synchronous rotation: Implications for fracturing on Europa, *Icarus*, *61*, 175–185.
- Hoppa, G. V., B. R. Tufts, R. Greenberg, and P. E. Geissler (1999), Formation of cycloidal features on Europa, *Science*, *285*, 1899–1902.
- Hopper, J. R., and W. R. Buck (1993), The initiation of rifting at constant tectonic force: Role of diffusion creep, *J. Geophys. Res.*, *98*(B9), 16,213–16,221.
- Hussmann, H., T. Spohn, and K. Wiczerkowski (2002), Thermal equilibrium states of Europa's ice shell: Implications for internal ocean thickness and surface heat flow, *Icarus*, *156*, 143–151.
- Kadel, S. D., F. C. Chuang, R. Greeley, and J. M. Moore (2000), Geological history of the Tyre region of Europa: A regional perspective on European surface features and ice thickness, *J. Geophys. Res.*, *105*(E9), 22,657–22,669.
- Kargel, J. S., and S. Pozio (1996), The volcanic and tectonic history of Enceladus, *Icarus*, *119*(2), 385–404.
- Kirk, R., and D. Stevenson (1987), Thermal evolution of a differentiated Ganymede and implications for surface features, *Icarus*, *69*, 91–134.
- Klinger, J. (1980), Influence of a phase transition of ice on the heat and mass balance of comets, *Science*, *209*, 271–272.
- Kruse, S., M. McNutt, J. Phipps-Morgan, and L. Royden (1991), Lithospheric extension near Lake Mead, Nevada: A model for ductile flow in the lower crust, *J. Geophys. Res.*, *96*(B3), 4435–4456.
- Kuznir, N. J., and R. G. Park (1987), The extensional strength of continental lithosphere: Its dependence on geothermal gradient, and crustal composition and thickness, in *Continental Extensional Tectonics*, edited by M. Coward, J. Dewey, and P. Hancock, *Geol. Soc. Spec. Publ.*, *28*, 35–52.
- Leith, A. C., and W. B. McKinnon (1996), Is there evidence for polar wander on Europa?, *Icarus*, *120*(2), 387–398.
- McKenzie, D. (1978), Some remarks on the development of sedimentary basins, *Earth Planet. Sci. Lett.*, *40*(1), 25–32.
- McKinnon, W. B. (1999), Convective instability in Europa's floating ice shell, *Geophys. Res. Lett.*, *26*(7), 951–954.
- Moore, J. M., et al. (1998), Large impact features on Europa: Results of the Galileo nominal mission, *Icarus*, *135*, 127–145.
- Newman, R., and N. White (1999), The dynamics of extensional sedimentary basins: Constraints from subsidence inversion, *Philos. Trans. R. Soc. London, Ser. A*, *357*(1753), 805–830.
- Nimmo, F. (2003), Non-Newtonian topographic relaxation on Europa, *Icarus*, in press.
- Nimmo, F., and E. Gaidos (2002), Strike-slip motion and double ridge formation on Europa, *J. Geophys. Res.*, *107*(E4), 5021, doi:10.1029/2000JE001476.
- Nimmo, F., and D. J. Stevenson (2001), Estimates of Martian crustal thickness from viscous relaxation of topography, *J. Geophys. Res.*, *106*, 5085–5098.
- Nimmo, F., R. T. Pappalardo, and B. Giese (2002), Effective elastic thickness and heat flux estimates on Ganymede, *Geophys. Res. Lett.*, *29*(7), 1158, doi:10.1029/2001GL013976.
- Nimmo, F., B. Giese, and R. T. Pappalardo (2003a), Estimates of Europa's ice shell thickness from elastically-supported topography, *Geophys. Res. Lett.*, *30*(5), 1233, doi:10.1029/2002GL016660.
- Nimmo, F., R. T. Pappalardo, and B. Giese (2003b), On the origins of band topography, Europa, *Icarus*, *166*, 21–32.
- O'Brien, D. P., P. Geissler, and R. Greenberg (2002), A melt-through model for chaos formation on Europa, *Icarus*, *156*(1), 152–161.
- Ojakangas, G. W., and D. J. Stevenson (1989), Thermal state of an ice shell on Europa, *Icarus*, *81*(1), 220–241.
- Pappalardo, R. T., S. J. Reynolds, and R. Greeley (1997), Extensional tilt blocks on Miranda: Evidence for an upwelling origin of Arden Corona, *J. Geophys. Res.*, *102*(E6), 13,369–13,379.
- Pappalardo, R. T., et al. (1998), Grooved terrain on Ganymede: First results from Galileo high-resolution imaging, *Icarus*, *135*, 276–302.
- Pappalardo, R. T., et al. (1999), Does Europa have a subsurface ocean? Evaluation of the geological evidence, *J. Geophys. Res.*, *104*(E10), 24,015–24,055.
- Parmentier, E. M., S. W. Squyres, J. W. Head, and M. L. Allison (1982), The tectonics of Ganymede, *Nature*, *295*, 290–293.
- Patel, J. G., R. T. Pappalardo, J. W. Head, G. C. Collins, H. Hiesinger, and J. Sun (1999), Topographic wavelengths of Ganymede groove lanes from Fourier analysis of Galileo images, *J. Geophys. Res.*, *104*(E10), 24,057–24,074.
- Press, W. H., S. A. Teukolsky, W. T. Vetterling, and B. P. Flannery (1992), *Numerical Recipes in Fortran*, Cambridge Univ. Press, New York.
- Prockter, L. M., J. W. Head III, R. T. Pappalardo, R. J. Sullivan, A. E. Clifton, B. Giese, R. Wagner, and G. Neukum (2002), Morphology of European bands at high resolution: A mid-ocean ridge-type rift mechanism, *J. Geophys. Res.*, *107*(E5), 5028, doi:10.1029/2000JE001458.
- Ranalli, G. (1995), *Rheology of the Earth*, Chapman and Hall, New York.
- Ruiz, J., and R. Tejero (2000), Heat flows through the ice lithosphere of Europa, *J. Geophys. Res.*, *105*(E12), 29,283–29,289.

- Schenk, P. (2002), Thickness constraints on the icy shells of the Galilean satellites from a comparison of crater shapes, *Nature*, *417*, 419–421.
- Schenk, P. M., and W. B. McKinnon (1989), Fault offsets and lateral crustal movement on Europa—Evidence for a mobile ice shell, *Icarus*, *79*(1), 75–100.
- Schenk, P. M., W. B. McKinnon, D. Gwynn, and J. Moore (2001), Flooding of Ganymede's bright terrains by low-viscosity water-ice lavas, *Nature*, *410*, 57–60.
- Showman, A. P., and R. Malhotra (1997), Tidal evolution into the Laplace resonance and the resurfacing of Ganymede, *Icarus*, *127*, 93–111.
- Solomatov, V. S., and L. N. Moresi (2000), Scaling of time-dependent stagnant lid convection: Application to small-scale convection on Earth and other terrestrial planets, *J. Geophys. Res.*, *105*(B9), 21,795–21,817.
- Stevenson, D. J. (2000), Limits on the variation of thickness of Europa's ice shell, *Lunar Planet. Sci.*, *XXXI*, abstract 1506.
- Sullivan, R., et al. (1998), Episodic plate separation and fracture infill on the surface of Europa, *Nature*, *391*, 371–372.
- Tufts, B. R., R. Greenberg, G. Hoppa, and P. Geissler (2000), Lithospheric dilation on Europa, *Icarus*, *146*(1), 75–97.
- Turcotte, D. L., and G. Schubert (1982), *Geodynamics*, John Wiley, Hoboken, N. J.
- Turtle, E. P., and B. A. Ivanov (2002), Numerical simulations of impact crater excavation and collapse on Europa: Implications for ice thickness, *Lunar Planet. Sci.*, *XXXIII*, abstract 1431.
- Zahnle, K., P. M. Schenk, H. F. Levison, and L. Dones (2003), Cratering rates in the outer solar system, *Icarus*, *163*(2), 263–289.
- 
- F. Nimmo, Department of Earth Sciences, University College London, Gower Street, London WC1E 6BT, UK. (nimmo@ess.ucla.edu)